A COMPETITIVE COMPARISON OF MULTIPARAMETER STACKING OPERATORS

J. Walda, B. Schwarz, and D. Gajewski

email: *jan.walda@uni-hamburg.de, benjamin.schwarz@earth.ox.ac.uk, dirk.gajewski@uni-hamburg.de*
keywords: *diffractions, CRS, multiparameter*

ABSTRACT

The classical common-midpoint stack, which sums along offsets, suffers in challenging environments where the acquisition is sparse. In the past, several multiparameter techniques were introduced that incorporate many neighboring common-midpoints in the stacking process. This increases data redundancy and reduces noise. Multiparameter methods that can be parametrized by the same wavefront attributes are the common-reflection-surface (CRS), implicit CRS, non-hyperbolic CRS and multifocusing. CRS-type operators use a velocity shift mechanism to account for heterogeneity. Multifocusing on the other hand uses a different mechanism: a shift of reference time. We formulate multifocusing such, that it uses the same mechanism as the CRS-type operators and compare them on a marine data set. In turn, we investigate the behavior of time-shifted versions of the CRS-type approximations. In order to provide fair comparison, we use a global optimization technique, differential evolution, which allows to accurately estimate a solution without initial bias. Our results show, that the velocity shift mechanism performs, in general, better than the one incorporating time shift. The non-hyperbolic operators are also less sensitive to the choice of aperture and perform better in the case of diffractions than conventional CRS, since diffractions are of higher order. Since the computational cost of non-hyperbolic CRS is almost the same as the one of conventional hyperbolic CRS but generally leads to a superior fit, we recommend its use in future.

INTRODUCTION

The common-midpoint (CMP) stack by Mayne (1962) has been successfully used for half a century and is still a common strategy. This method is very robust in most cases but does not perform well in noisy data. Alternative methods which use more traces to utilize data redundancy and reduce noise have been proposed over the last two decades. Some of those can be parametrized with the same attributes. In this work we focus on four multiparameter stacking approaches: multifocusing (MF, Gelchinsky et al., 1999; Landa et al., 2010), the common-reflection-surface (CRS) stack (Jäger et al., 2001), non-hyperbolic CRS (nCRS, Fomel and Kazinnik, 2013) and implicit CRS (iCRS, Schwarz et al., 2014). These stacking approaches can all be expressed in terms of three wavefront attributes (Hubral, 1983) but differ in their mathematical expression. Comparisons between these methods have been done in the past (e.g., Dell et al., 2013; Schwarz et al., 2015). However, some promising stacking methods were not included in these previous studies. Dell et al. (2013) compared the CRS variants using a normal-moveout (NMO) velocity guide function to estimate the attributes. In their study conflicting dips, which often are mainly caused by diffractions, are not carefully accounted for. It was shown that double-square-root operators perform better for diffraction events. Due to their comparably low amplitudes diffractions are often masked by stronger primary reflections. The full potential of higher-order CRS-type approximations can therefore not be revealed, when conflicting dips are not properly treated. In addition, although a quantitative comparability is generally difficult to achieve, a comparison of the computational efficiency, thus far, has not been addressed in this context.

Schwarz et al. (2015) introduced a new parametrization for CRS-type stacking operators in terms of time and velocity shifts. multifocusing, in contrast to all other approaches, utilizes a different mechanism, a time shift, to perturb the moveout, whereas the other methods shift the velocity in order to account for overburden heterogeneity. Schwarz et al. (2015) also introduced a recipe to translate time shifts into velocity shifts and vice versa, which allows the comparison of all the operators in the same domain. However, in this study the authors used a synthetic model and estimated attributes based on an initial solution obtained by the so called pragmatic approach (Jäger et al., 2001) which can be inaccurate for complex geology (Walda and Gajewski, 2015).
Since in all previous studies, hyperbolic and higher-order CRS expressions including multifocusing were formulated in terms of the two aforementioned mechanisms, they were not compared on common ground, i.e., the gained results are hard to appreciate. In this work, we present an unbiased comparison of the double-square-root operators and conventional hyperbolic CRS for both possible mechanisms consistently, using a global optimization scheme and sophisticated conflicting dip processing on a strongly scattering industrial field data set.

MULTIPARAMETER STACKING

The CMP method stacks data along a traveltime curve in offset direction

$$S(t_0, m_0) = \iint P(t(t_0, h), m_0, h)dh \quad . \tag{1}$$

This method uses only data redundancy in offset direction which becomes problematic if only few traces are available. Challenging data, where CMP processing does not produce desired results, benefit from stacking techniques where the summation is carried out in offset and midpoint direction

$$S(t_0, m_0) = \iint P(t(t_0, \Delta m, h), m, h)dmdh \quad . \tag{2}$$

In Equation 2, the quantity $\Delta m = m_0 - m$ is the midpoint displacement. Since neighboring midpoints m are stacked into the midpoint m_0 as well, a higher amount off traces are summed which results in a better signal-to-noise ratio. However, the traveltime description depends on more parameters compared to classical CMP stacking. Hubral (1983) introduced wavefront attributes that can be used as a parametrization to describe the required traveltime surface $t(t_0, \Delta m, h)$ shown in Figure 1. Traveltime operators that use these attributes can be classified as common-reflection-surface (CRS) type operators. They differ in their mathematical structure which stem from the underlying assumptions. While CRS itself is a hyperbolic single-square-root traveltime expression, the other three introduced in the following sections are double-square-root operators.

Multifocusing

Planar multifocusing introduced by Gelchinsky et al. (1999) and revisited by Landa et al. (2010) attempts to express the traveltime in terms of the traveltime of a central ray and two corrections at the source and receiver position from a paraxial ray. To achieve this, a parameter to focus the NIP and N wave for a planar reflector is required which reads

$$R^{\pm} = \frac{1 \pm \gamma}{\frac{1}{R_N} \pm \frac{\gamma}{R_{NIP}}} \quad , \tag{3}$$

$$\gamma = \frac{\Delta x_s - \Delta x_g}{\Delta x_s + \Delta x_g + 2\frac{\sin\alpha}{R_{NIP}}\Delta x_s \Delta x_g} \quad , \tag{4}$$

where $\Delta x_s = \Delta m - h$ and $\Delta x_g = \Delta m + h$. The quantity γ is called focusing parameter, which together with the equation

$$\begin{aligned} t(\Delta m, h) = t_0 &+ \frac{1}{v_0}\sqrt{(R^+)^2 + 2R^+\Delta x_s \sin\alpha + (\Delta x_s)^2} \\ &+ \frac{1}{v_0}\sqrt{(R^-)^2 + 2R^-\Delta x_g \sin\alpha + (\Delta x_g)^2} - \frac{R^+ + R^-}{v_0} \quad , \end{aligned} \tag{5}$$

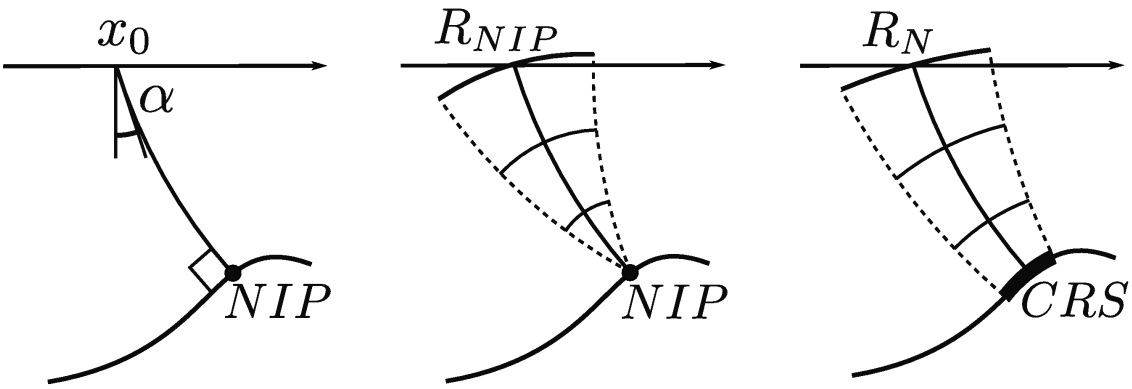

Figure 1: Two hypothetical experiments: The normal-incidence-point wave is shown in the middle with its radius of curvature R_{NIP}. The normal wave with the radius of curvature R_N, is caused by an exploding reflector experiment (right). Both have the angle of emergence α (left).

leads to the multifocusing operator. However, multifocusing as presented here and in literature uses a time shift to account for heterogeneity. Therefore, previous comparisons of multifocusing with other CRS type operators as in (Tygel et al., 1999; Landa et al., 2010; Fomel and Kazinnik, 2013) are not on common ground.

Common-reflection-surface

The CRS stack is a multiparameter stacking technique (Müller, 1999; Mann et al., 1999; Jäger et al., 2001; Mann, 2002) that considers neighboring midpoints as well as the offset (see Figure 2) while the CMP method uses only offsets. It describes an event in the vicinity of the zero-offset sample by a second-order traveltime approximation. Since more traces are stacked, the signal-to-noise ratio is improved significantly.

The CRS operator is formulated in terms of three wavefront attributes, which are related to two hypothetical one-way experiments as illustrated in Figure 1. The resulting two waves are described by the angle of emergence α of the zero-offset ray and the corresponding radii of curvature: R_N for the normal (N) wave and R_{NIP} for the normal-incidence-point (NIP) wave (Hubral, 1983). The N wave is generated by a fictitious exploding reflector experiment around the normal-incidence-point. The NIP wave is generated by a fictitious point source placed at the normal-incidence-point.

Using the notation by Fomel and Kazinnik (2013), the CRS formula in its hyperbolic expression can be written as

$$t(t_0, \Delta m, h) = \sqrt{F(\Delta m, t_0) + b_2 h^2} \quad , \tag{6}$$

$$F(t_0, \Delta m) = (t_0 + a_1 \Delta m)^2 + a_2 \Delta m^2 \quad . \tag{7}$$

The coefficients a_1, a_2 and b_2 can be related to the wavefront attributes α, R_{NIP} and R_N as

$$\begin{aligned} a_1 &= \frac{2 \sin \alpha}{v_0} \\ a_2 &= \frac{2 t_0 \cos^2 \alpha}{v_0 R_N} \\ b_2 &= \frac{2 t_0 \cos^2 \alpha}{v_0 R_{NIP}} \quad . \end{aligned} \tag{8}$$

The quantity v_0 is the near surface velocity.

Non-hyperbolic common-reflection-surface

Fomel and Kazinnik (2013) introduced another extension of the conventional CRS approach. In contrast to iCRS the non-hyperbolic common-reflection-surface (nCRS) method assumes a hyperbolic reflector since

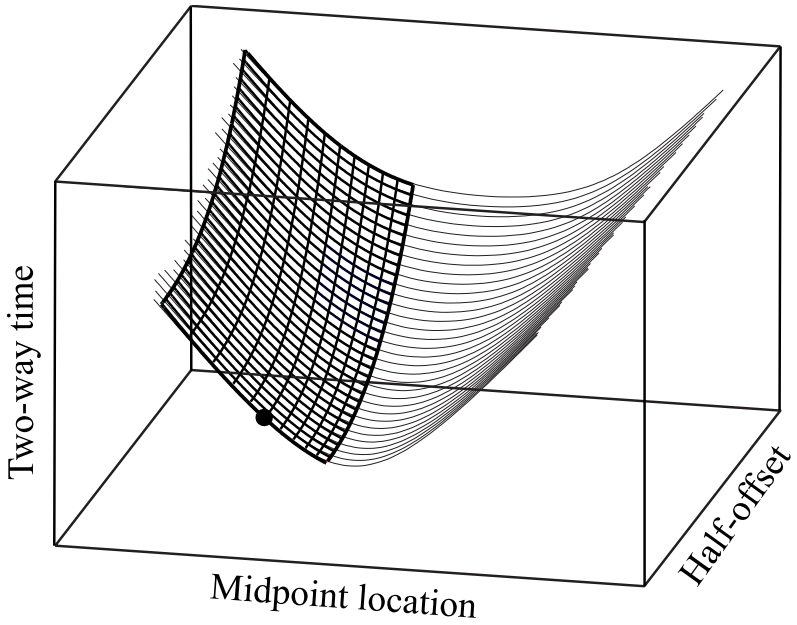

Figure 2: The CRS method stacks along the fat black traveltime surface and assign the value to the black dot.

there is no closed form solution for a circular reflector. This requires additional iterations to estimate the reflection point angle θ for the iCRS operator. The nCRS does not need this iterations and therefore saves computation time.

The nCRS operators reads

$$t(t_0, \Delta m, h) = \sqrt{\frac{F(t_0, \Delta m) + ch^2 + \sqrt{F(t_0, \Delta m - h)F(t_0, \Delta m + h)}}{2}} \quad , \tag{9}$$

where F is defined according to Equation 7 and $c = 2b_2 + a_1^2 - a_2$ accounts for the asymmetry of the source-receiver traveltime contributions. From an implementation point of view, it requires very few additional computations compared to CRS (see Equation 6) which makes it very easy and efficient to implement in existing CRS codes. Furthermore, calculating the second square root is not as problematic since most quantities can be calculated before.

Implicit common-reflection-surface

The implicit common-reflection-surface (iCRS) stack is a further development of the common-reflection-surface (CRS) stack. In contrast to the conventional CRS technique, iCRS assumes a circular reflector in the subsurface.

The iCRS operator is another multiparameter stacking technique derived by Schwarz et al. (2014). It assumes a locally circular reflector as shown in Figure 3. It depends on three parameters of the circle (x_c, H and R) as well as the background velocity of the medium V and reads

$$\begin{aligned} t_s(\Delta m, h) &= \frac{1}{V}\sqrt{(\Delta m - h - \Delta x_c - R\sin\theta)^2 + (H - R\cos\theta)^2} \quad , \\ t_g(\Delta m, h) &= \frac{1}{V}\sqrt{(\Delta m + h - \Delta x_c - R\sin\theta)^2 + (H - R\cos\theta)^2} \quad , \\ t(\Delta m, h) &= t_s(\Delta m, h) + t_g(\Delta m, h) \quad , \end{aligned} \tag{10}$$

where θ is the reflection point angle on the circle and Δx_c the displacement of the circle relative to the central midpoint location m_0. The reflection angle θ on the circle has to be calculated additionally. It

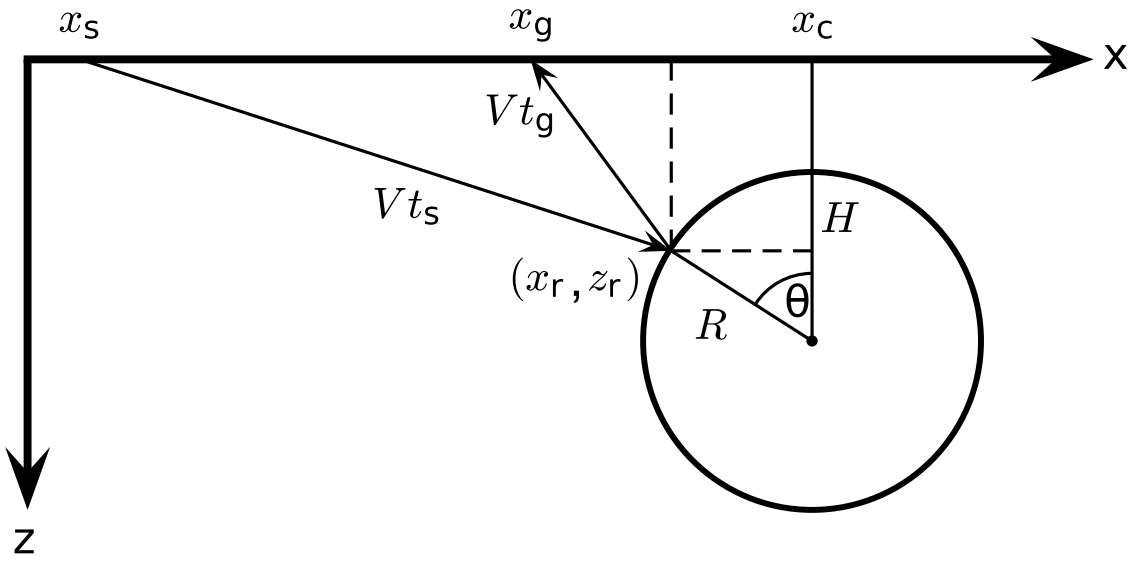

Figure 3: Geometrical deviation of the iCRS operator.

depends on the traveltimes t_s and t_g

$$\tan\theta = \tan\theta_0 + \frac{h}{H}\frac{t_s - t_g}{t_s + t_g} \tag{11}$$

and can be solved in an iterative fashion with a first guess provided by a zero-offset ray. In this case, the dependence on t_s and t_g vanishes

$$\tan\theta_0 = \frac{\Delta m - \Delta x_c}{H} \quad . \tag{12}$$

Schwarz et al. (2014) showed that a single iteration is already sufficient to achieve an accurate fit in heterogeneous media. The parameters of the circle can be related to the CRS wavefront attributes by

$$\begin{aligned}
V_{NMO} &= \sqrt{\frac{2v_0 R_{NIP}}{t_0 \cos^2\alpha}} \\
V &= \frac{V_{NMO}}{\sqrt{1 + \frac{V_{NMO}^2}{v_0^2}\sin^2\alpha}} \\
\Delta x_c &= \frac{-R_{NIP}\sin\alpha}{\cos^2\alpha\left(1 + \frac{V_{NMO}^2}{v_0^2}\sin^2\alpha\right)} \\
H &= \frac{v_0 R_{NIP}}{V_{NMO}\cos^2\alpha\left(1 + \frac{V_{NMO}^2}{v_0^2}\sin^2\alpha\right)} \\
R &= \frac{\frac{v_0 R_N}{V_{NMO}\cos^2\alpha} - \frac{V_{NMO}t_0}{2}}{\sqrt{1 + \frac{V_{NMO}^2}{v_0^2}\sin^2\alpha}} \quad .
\end{aligned} \tag{13}$$

Therefore, the iCRS traveltime surface can be written in terms of the CRS wavefront attributes α, R_{NIP} and R_N.

TIME SHIFT AND VELOCITY SHIFT

All presented approximations describe paraxial traveltimes and are functions of the same wavefront attributes

$$t = t(\alpha, R_{NIP}, R_N). \tag{14}$$

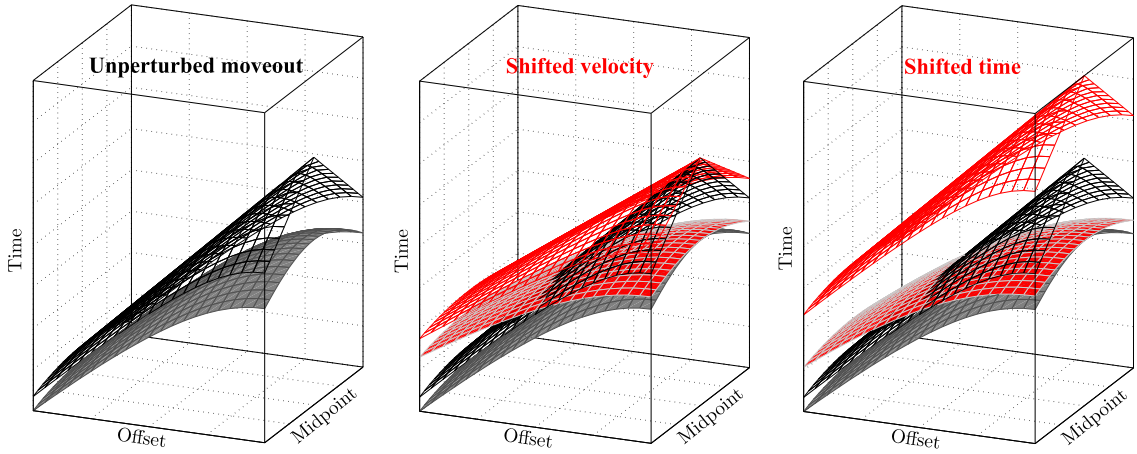

Figure 4: Illustration of the two possible mechanisms to perturb the moveout to account for overburden heterogeneity. The solid line represent the actual unperturbed (black) and perturbed (red) moveout. For the velocity shift, the slope of the moveouts asymptote (meshed) is changed. In case of the time shift, the time of origin of the asymptote is changing.

In the recent work of Schwarz et al. (2015), the authors showed that the multifocusing moveout, despite being parametrized in terms of the same kinematic wavefront attributes, behaves differently from all other approaches when heterogeneity is present. In this study they found, that a time shift is responsible for perturbing the moveout, whereas for the moveout of CRS-type operators, a velocity shift accounts for velocity changes in the overburden. In Figure 4 the conceptual difference between either shifting the time or the velocity is illustrated. Schwarz et al. (2015) introduced a simple recipe to transform time shifts to velocity shifts and vice versa,

$$\frac{1}{v_{shift}^2} = \left(\frac{\sin\alpha}{v_0}\right)^2 + \frac{t_0}{t_{shift}}\left(\frac{1}{v_0^2} - \left(\frac{\sin\alpha}{v_0}\right)^2\right) \quad , \tag{15}$$

where v_0 is the near surface velocity, t_0 the zero-offset reference traveltime and $t_{shift} = 2R_{NIP}/v_0$ the shifted zero-offset traveltime. Equation 15 connects both parametrizations. The time shift mechanism can be illustrated in the framework of geometrical optics and since the dip is naturally accounted for, Equation 15 can be considered as a generalized osculating equation (see De Bazelaire, 1988). This allows to freely choose the desired mechanism to account for heterogeneity. However, this also means each operator introduced in literature has two versions. Four CRS type operators are available in literature, namely multifocusing (MF, Gelchinsky et al., 1999; Landa et al., 2010), CRS (Jäger et al., 2001), non-hyperbolic CRS (nCRS) introduced by Fomel and Kazinnik (2013) and implicit CRS (iCRS, Schwarz et al., 2014). This means there is a choice of eight CRS type traveltime expressions that can be used in Equation 2. In order to evaluate differences in the practical application we apply all operators under the same conditions to marine industrial field data. This means we use the global optimization technique differential evolution to estimate the CRS wavefront attributes with the same aperture for all approximations. Furthermore, we do not use a velocity guide function to better evaluate the performance differences of the operators. A guide function would otherwise introduce a favorable or unfavorable bias, since velocities might differ, depending on the operator. Since the strongest differences are expected for diffractions, we also account for conflicting dips by dividing the α search space into small cluster. This allows to recognize different events in separate α cluster (Walda and Gajewski, 2015).

MARINE DATA EXAMPLE

In order to find the most suited operator, especially for diffraction imaging, their performance under the very same conditions, as described above, are compared. The sole difference is the operator used for traveltime fitting to calculate the semblance.

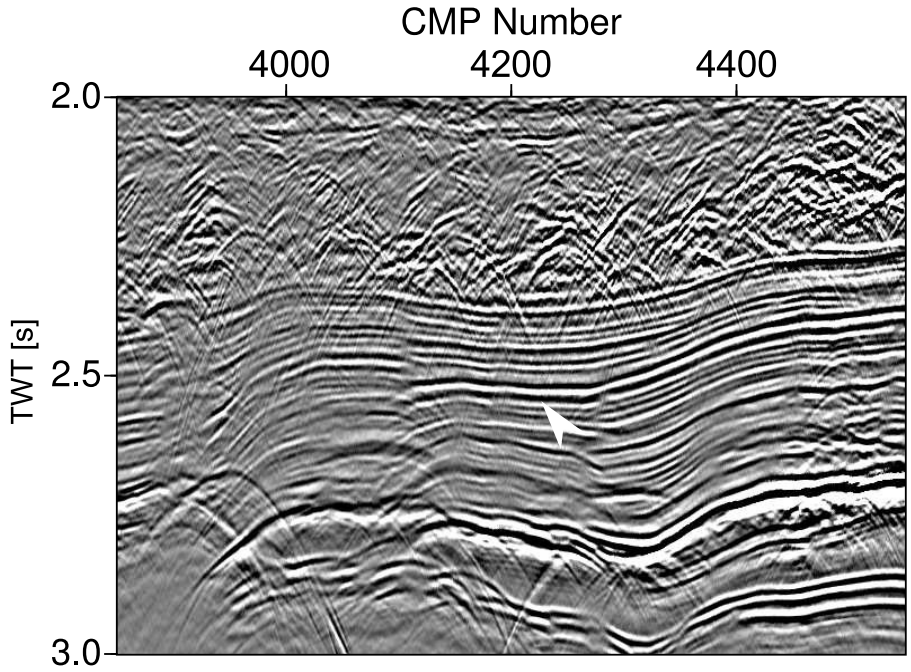

Figure 5: Stacked section in the north east of the profile. The arrow indicates the location of the sample where the objective function is investigated.

A method to gain more insight on the behavior of the operators and how they shape the objective function is to calculate the objective function for a specific test case. For that purpose, for a test sample shown by the arrow in Figure 5, the α-R_{NIP} planes for a constant R_N of every operator is plotted in Figure 6. The midpoint aperture is 800 m and the target-offset ratio approximately 2:1. The color-coded semblance is clipped to show the diffractions, since the reflection has a much higher semblance. Since this is far beyond the hyperbolic limit, the CRS operator cannot fit the diffractions anymore and they are hardly recognizable. Furthermore, the estimated attributes differ as well as the general shape of the objective function. This is not so much the case for the higher-order operators multifocusing, iCRS and nCRS. They do not differ at the event location, only further away in the noisy part of the objective function.

A comparison of the fitted semblance value allows to evaluate how successful the operators fitted the data. Since every operator has its velocity and time shifted version, it is necessary to investigate which representation is better suited for stacking. Figure 7 shows the semblance of velocity-shifted nCRS as a reference and the difference plots of three exemplarily chosen operators. In the difference plots, a red color represents higher semblance values for the velocity-shifted version whereas blue colors show higher semblance for the time-shifted operator. Independent of the actual traveltime expression, the velocity-shifted versions show a higher coherence almost everywhere and a better fit for the same events.

Figure 8 shows the semblance obtained by nCRS and the respective difference plots of nCRS and the other operators in their velocity-shifted version. Red colors represent a better fit for nCRS, blue colors for CRS, iCRS or multifocusing. The difference plots of nCRS minus iCRS and nCRS minus multifocusing show no significant differences. In terms of accuracy they perform similarly on the marine field data. However, they show differences compared to the hyperbolic CRS represented by the difference plot of nCRS minus CRS. Differences for reflections are not visible, which is not surprising, because all considered expressions coincide up to second order. In case of diffractions, mainly red colors appear which means a better fit for nCRS. This is no surprise because diffractions are higher order phenomena. Since the differences of nCRS to iCRS and multifocusing are almost nonexistent, the differences are the same for all non-hyperbolic operators compared to hyperbolic CRS. The fit of diffractions is better for non-hyperbolic operators. This also shows in the estimated attributes, exemplarily shown for the moveout velocity in Figure 9. A reference velocity field, estimated using nCRS and difference plots of nCRS minus CRS, iCRS and

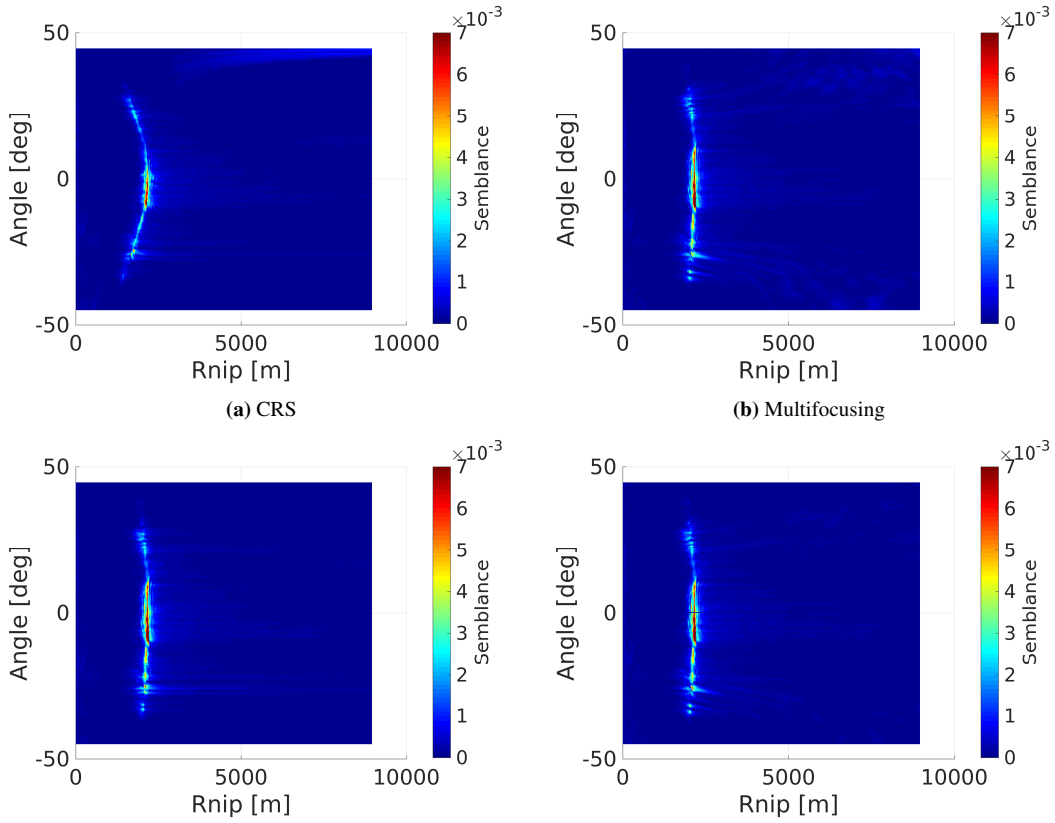

(a) CRS **(b)** Multifocusing

(c) nCRS **(d)** iCRS

Figure 6: Objective functions of (a) CRS, (b) multifocusing, (c) nCRS and (d) iCRS for the sample shown by an arrow in Figure 5. The offset-target ratio is 2.0 which exceeds the hyperbolic limit significantly. Therefore, the objective function of the conventional CRS operator differs severely from the non-hyperbolic variants. The difference between the individual non-hyperbolic expressions however, is negligible.

multifocusing are shown. Red colors show a higher moveout velocity of nCRS while blue colors indicate higher moveout velocities for the other operators. The biggest differences are visible for nCRS minus CRS. In case of diffractions, CRS shows higher moveout velocities close to the apex while at the diffraction tail, the approximation of nCRS leads to higher moveout velocities, which seems more accurate because the semblance of nCRS is higher. nCRS and multifocusing show very similar moveout velocities apart from areas of very low coherence. Interestingly, even though the differences in the coherence between nCRS and iCRS are almost nonexistent, the moveout velocities show small differences. For dipping events, the moveout velocity of iCRS is higher than for nCRS. Unfortunately it is hard to tell, which is more accurate. Therefore, the obtained velocities should be used carefully.

The observation, that non-hyperbolic operators perform better in case of diffractions than hyperbolic CRS when diffractions are concerned, is further supported by a diffraction separation shown in Figure 10. An excerpt of a diffraction separation using nCRS and CRS is compared. The excerpt area is highlighted by the red box. In case of nCRS, more diffractions become visible and are imaged more continuously. The arrows highlight diffractions where this can be observed in particular.
Figure 11 shows a comparison of the computational cost of the compared operators. The additional computational overhead of the velocity-shifted nCRS is very small (about 5 %) while the better accuracy for diffractions and lower sensitivity with respect to the aperture are strong benefits. Depending on the task, nCRS, in our complex field data example, provides the best trade-off between accuracy, stability and computational effort.

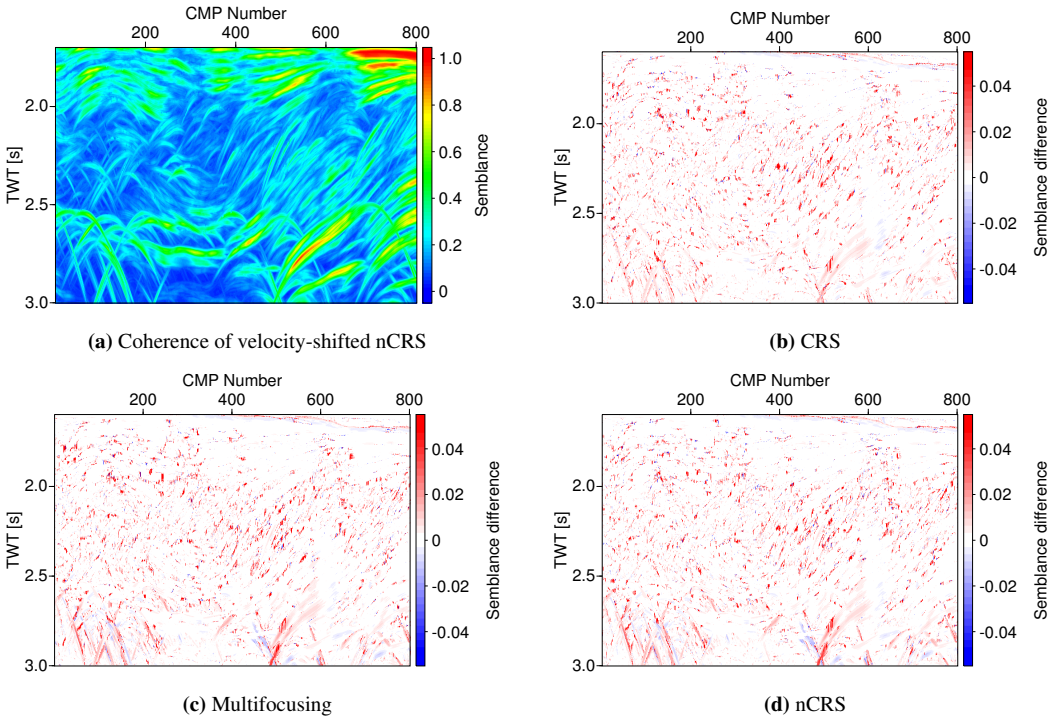

(a) Coherence of velocity-shifted nCRS

(b) CRS

(c) Multifocusing

(d) nCRS

Figure 7: Semblance section obtained by (a) the velocity-shifted nCRS operator and difference plots of velocity-shifted operators to their time shifted counterparts for (b) CRS, (c) multifocusing and (d) nCRS. A red color indicates a higher semblance for the velocity-shifted operator, while blue colors indicate a better semblance of time shifted operators.

DISCUSSION

We have compared multiparameter operators that can be parametrized by the same wavefront attributes. Since the major difference of the quality of the fit is due to the single-square-root and double-square-root expression rather than the used operator, we think we should focus the research into another direction instead of developing new approximations. The results show, that there is practically no difference in the actual application between multifocusing, nCRS and iCRS. This requires to formulate multifocusing such that it uses the same mechanism to account for heterogeneity as CRS-type operators. The recipe to transform multifocusing to a velocity-shifted formulation and the CRS variants to a time-shifted version, in our opinion, leads to an unification where the differentiation is rather due to the single-square-root and double-square-root. In future it might be better to refer to those as approximation of the CRS family.

Since CRS and nCRS are also available in 3D in literature, there are strong arguments to use nCRS in future, since its a double-square-root approximation and outperforms the single-square-root in terms of accuracy and uses less computational time than the other double-square-root expressions.

CONCLUSIONS

We investigated available multiparameter stacking operators from literature, that can be parametrized by the CRS wavefront attributes. Our results show, that in general a non-hyperbolic operator should be used rather than the hyperbolic CRS. They generally provide a better fit and depend less on the choice of the stacking aperture. The question which specific operator should be used in terms of accuracy cannot be answered since multifocusing, iCRS and nCRS perform similarly in that respect. However, in our global optimization scheme nCRS uses less computation time since the semblance evaluation is not as expensive as in iCRS and multifocusing. Those require additional computations such as the focusing parameter or calculation of the reflection angle on the sphere.

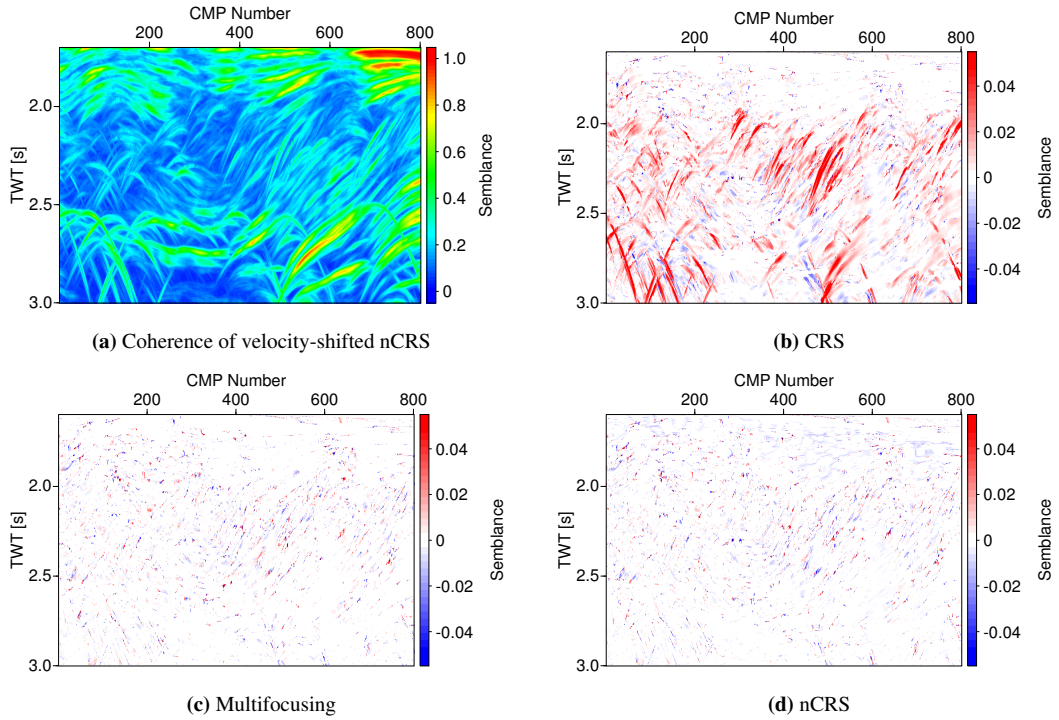

(a) Coherence of velocity-shifted nCRS

(b) CRS

(c) Multifocusing

(d) nCRS

Figure 8: Semblance section obtained by (a) the velocity-shifted nCRS operator and difference plots of velocity-shifted nCRS to the other velocity-shifted CRS-type operators: (b) CRS, (c) multifocusing and (d) iCRS. A red color indicates a higher semblance for the velocity-shifted nCRS operator, while blue colors indicate a better semblance the other velocity-shifted operator.

Every operator can be formulated in terms of a velocity or a time shift. The comparison shows that velocity-shifted versions perform better computationally and lead to a more accurate fit. Since multifocusing up to this point appeared in the time shifted version in literature, it is recommended to transform it into its velocity-shifted version to obtain a better performance. However, velocity-shifted nCRS provides the best trade-off between accuracy and computational cost.

ACKNOWLEDGMENTS

The work was supported by the sponsors of the Wave Inversion Technology (WIT) consortium. The marine data was provided by TGS-NOPEC. We would like to thank the Applied Seismics Group Hamburg for continuous discussions.

REFERENCES

De Bazelaire, E. (1988). Normal moveout revisited: Inhomogeneous media and curved interfaces. *Geophysics*, 53(2):143–157.

Dell, S., Downes, J., and Hertweck, T. (2013). Comparison of Non-hyperbolic and Standard CRS Using Complex Field Data. *2013 SEG Annual Meeting*, pages 4357–4361.

Fomel, S. and Kazinnik, R. (2013). Non-hyperbolic common reflection surface. *Geophysical Prospecting*, 61(1):21–27.

Gelchinsky, B., Berkovitch, A., and Keydar, S. (1999). Multifocusing homeomorphic imaging: Part1. Basic concepts and formulas. *Journal of Applied Geophysics*, 42(3-4):229–242.

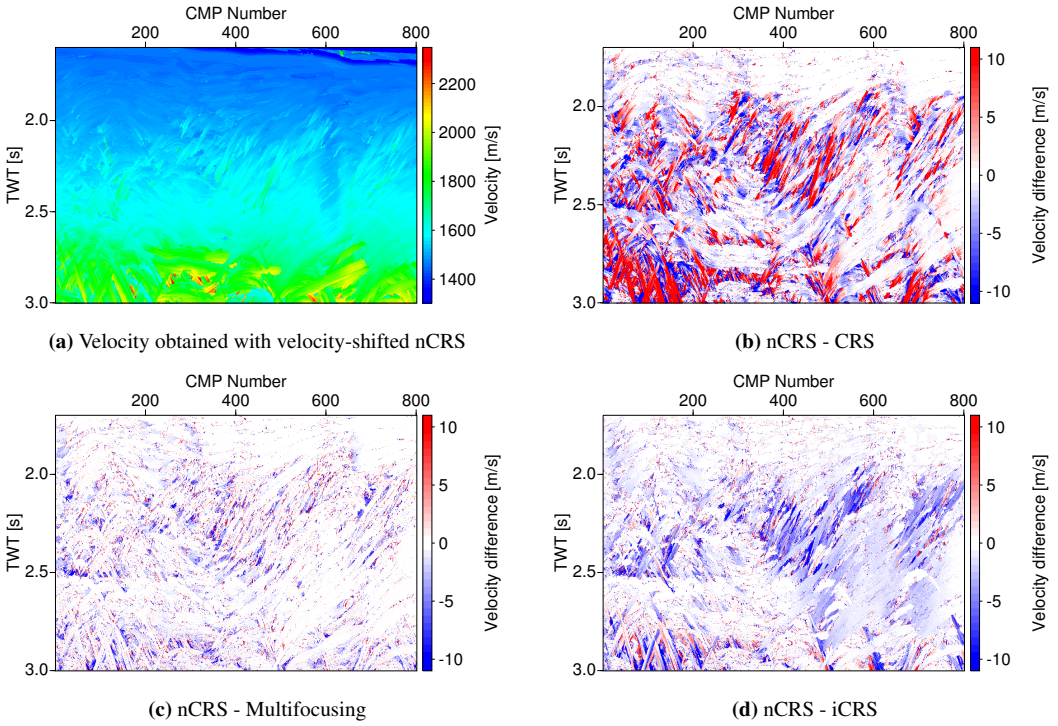

(a) Velocity obtained with velocity-shifted nCRS

(b) nCRS - CRS

(c) nCRS - Multifocusing

(d) nCRS - iCRS

Figure 9: Comparison of the estimated moveout velocities obtained by the different operators. The results from nCRS serve as reference for difference plots, since the differences are small. A red colour indicates a velocity for the velocity-shifted nCRS operator, while blue colors indicate a lower velocity compared to the other velocity-shifted operator.

Hubral, P. (1983). Computing true amplitude reflections in a laterally inhomogeneous earth. *Geophysics*, 48:1051–1062.

Jäger, R., Mann, J., Höcht, G., and Hubral, P. (2001). Common-reflection-surface stack: Image and attributes. *Geophysics*, 66:97–109.

Landa, E., Keydar, S., and Moser, T. J. (2010). Multifocusing revisited-inhomogeneous media and curved interfaces. *Geophysical Prospecting*, 58(6):925–938.

Mann, J. (2002). *Extensions and Applications of the Common-Reflection-Surface Stack Method*. PhD thesis, Logos Verlag, Berlin.

Mann, J., Jäger, R., Müller, T., Höcht, G., and Hubral, P. (1999). Common-reflection-surface stack - a real data example. *Journal of Applied Geophysics*, 42:301–318.

Mayne, W. H. (1962). Common reflection point horizontal data stacking techniques. *Geophysics*, 27(6):927–938.

Müller, T. (1999). *The Common Reflection Surface Stack Method: Seismic Imaging without explicit knowledge of the velocity model*. PhD thesis, University of Karlsruhe.

Schwarz, B., Vanelle, C., and Gajewski, D. (2015). Shifted Hyperbola Revisited-The Two Faces of NMO. *77th EAGE Conference and Exhibition 2015*.

Schwarz, B., Vanelle, C., Gajewski, D., and Kashtan, B. (2014). Curvatures and inhomogeneities: An improved common-reflection approach. *Geophysics*, 79(5):S231–S240.

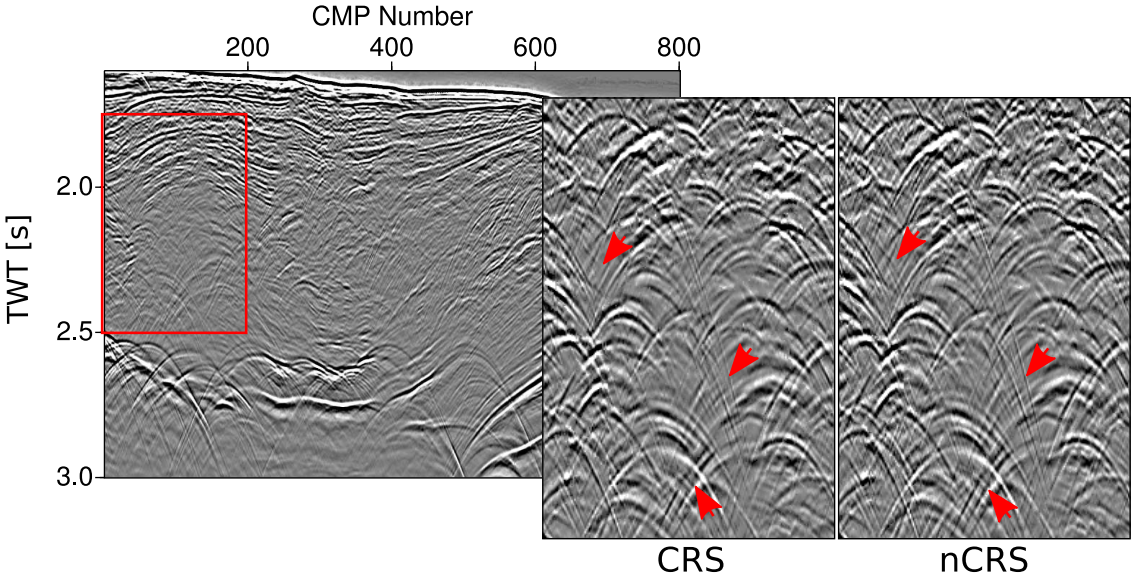

Figure 10: Stacked section of the fault system. The red box shows the excerpt shown on the right, where a diffraction separation is performed using attributes obtained by the CRS and nCRS operators. Red arrows indicate improvements achieved by nCRS compared to CRS. multifocusing and iCRS are not shown since they performed similar to nCRS.

Tygel, M., Santos, L. T., and Schleicher, J. (1999). Multifocus moveout revisited: derivations and alternative expressions. *Journal of Applied Geophysics*, 42(3-4):319–331.

Walda, J. and Gajewski, D. (2015). Common-reflection-surface stack improvement by differential evolution and conflicting dip processing. *SEG Technical Program Expanded Abstracts*, pages 3842–3847.

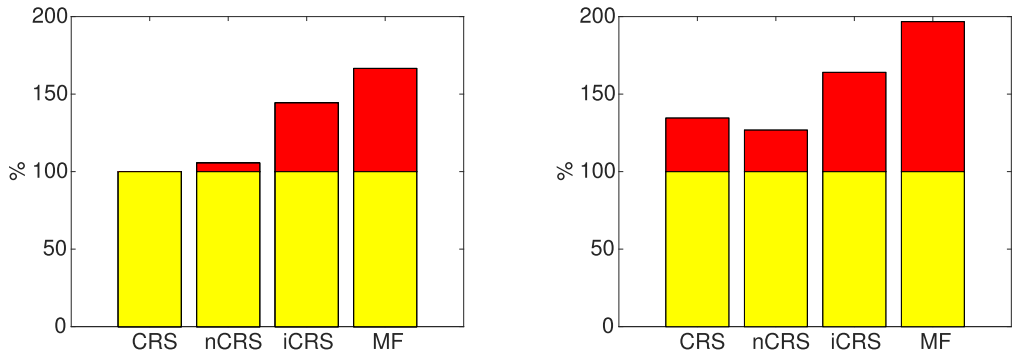

(a) Velocity-shifted

(b) Time-shifted

Figure 11: Comparison of the computation time for each operator in their velocity (a) and time-shifted version (b). The hyperbolic CRS in the velocity-shifted version is the reference (100 %). The yellow color represents the calculation time of CRS while the red color is the additional computational cost of the corresponding operator.